Heliyon 7 (2021) e05842

Contents lists available at ScienceDirect

Heliyon

journal homepage: www.cell.com/heliyon

Research article

Adaptive moving mesh algorithm based on local reaction rate

Viktória Koncz [a,*], Ferenc Izsák [b], Zoltán Noszticzius [a], Kristóf Kály-Kullai [a]

[a] Department of Physics, Budapest University of Technology and Economics, 1521 Budapest, Hungary
[b] Department of Applied Analysis and Computational Mathematics, MTA ELTE NumNet Research Group, Eötvös University, 1518 Budapest, Hungary

ARTICLE INFO

Keywords:
Adaptive FEM
Moving mesh
Reaction-diffusion systems
Acid-base diode
COMSOL Multiphysics

ABSTRACT

An empirical mesh adaption algorithm is introduced for modeling one-dimensional reaction-diffusion systems with large moving gradients. Our new algorithm is based on the revelation, that in reaction-diffusion systems the high moving concentration gradients appear nearby to the region where the rate of reaction is maximal, thus the local reaction rate can be used to control the mesh adaption. We found, that the main advantage of such a method is its simplicity and easy implementation. As an example we study an acid-base diode, where large moving gradients appear. The mathematical model of the diode contains several parabolic PDEs, coupled with one elliptic PDE. An *r*-refinement technique is used and attached to the commercial finite element solver COMSOL. We investigated the time-dependent salt effects of the diode with our developed algorithm. Our mesh adaption method is advantageous for modeling of any reaction-diffusion systems with localized high concentration gradients.

1. Introduction

Acid-base diodes, which are complex reaction-diffusion-ionic migration systems, could theoretically be used as ion-sensors. They could even form parts of so-called lab on a chip electroanalytical devices because of their simplicity. We would like to materialize such sensors as our final aim. To achieve this aim, it is important to study and model the time evolution of the effects, which would be the basis of their application as ion sensor.

In an electrolyte diode a hydrogel cylinder connects an alkaline and an acidic reservoir. This way diffusion, migration and reaction of the components are allowed, but advection and convection are restrained, unlike in pure water. Due to the applied electric potential between the edges of the gel cylinder, hydrogene (H^+) and hydroxil (OH^-) ions can get inside the connecting element, where water is formed from their reaction.

It means, that somewhere in the modeled domain there is a reaction zone, where this chemical acid-base reaction occurs. This reaction zone is characterized by large concentration and potential gradients. Dynamical simulations of transient behavior in such systems can be difficult due to the large moving gradients of the model variables (concentration and potential). The modeled reaction-diffusion system is described by a set of parabolic partial differential equations (PDEs, in this case mass balance equations for the chemical components) and one elliptic partial differential equation (Poisson-equation).

After the spatial discretization of the domain a system of ordinary differential equations is obtained, which is integrated forward by time numerically (method of lines). Regardless the spatial discretization method (e.g. finite difference method, finite element method) the applied mesh has special impact on the numerical solvability, speed of convergence, and approximation error. The higher the number of grid points used, the smaller the error will be. However, having a dense grid is computationally expensive, demanding a large chunk of memory and an extended runtime (Farmaga et al., 2011, Zimmerman, 2006). If the solutions have regions of high spatial activity, a standard uniform fixed-grid technique is computationally inefficient, since to afford an accurate numerical approximation and reach convergence, it should contain, in general, a very large number of grid points. The mesh needs to be locally refined. Moreover, if the regions of high spatial activity are moving in time, like steep moving fronts in reaction-diffusion systems, then the mesh should be adapted accordingly.

Regarding to the spatial grid adaption strategies, at least three different methods can be distinguished:

- *r*-refinement or the moving mesh (relocation) method: in this case fixed number of grid points is used, and the positions of points move.

* Corresponding author.
E-mail address: viki.koncz@gmail.com (V. Koncz).

https://doi.org/10.1016/j.heliyon.2020.e05842
Received 2 October 2020; Received in revised form 19 November 2020; Accepted 21 December 2020

- *h*-refinement or the local refinement method: the number of grid points is not fixed. Points are added to or removed from the grid, according to the local requirements, the original grid points stay in the same location. Practically, the spatial grid step h is locally decreased or increased.
- *p*-refinement: in this approach a fixed mesh is used, and the polynomial degree of basis (p) alters.

Certainly, the combination of these methods exists (Schwab, 1999). Although the moving mesh method has been less popular than the local refinement method, which is due to the difficulty of deriving suitable governing equations for the adaptive mapping, it has some useful features in numerical computations. E.g. it is easy to implement, and couple to any fixed mesh software, and difficulties from the change in number of grid points can be avoided (Přibyl et al., 2006).

Usually the moving mesh methods are based on the equidistribution principle (Huang et al., 1994), meaning selecting mesh points in such a way, that an empirical error is equalized over each subinterval on the mesh. The error distribution is followed by a monitor function, which is derived from the first and second derivatives of dependent variables. (Often this does not resemble to numerical errors.)

In the literature there are many examples about the successful numerical modeling of similar PDEs like the ones describing the behavior of the diode. Most of the methods require the complete development and full implementation of the spatial discretization and time integration of the model equations. A moving mesh method was developed (Zegeling and Kok, 2004) to solve the equations of reaction-diffusion systems, namely the Gray-Scott and Brusselator models. A system of adaptive mesh PDEs describing the mesh movement is set up and solved (in this case decoupled from the original PDE system), in fact the solution is the realization of a coordinate transformation between physical and computational coordinates. The adaptive mesh PDEs are derived from the minimization of a so-called mesh-energy functional. The variational approach of the moving mesh methods is general (Cao et al., 2003). Usually the original PDEs are coupled with the mesh PDEs (Zegeling and Keppens, 2001). More examples about an *r*-method are found in (Coimbra et al., 2004), (Zegeling and Blom, 1992).

An *h*-method was developed for solving electrochemistry problems with large spatial gradients applying a finite difference method (Bieniasz, 2000). Later this method was successfully used for the simulation of the Nernst-Planck-Poisson equations and Nernst-Planck equation with the assumption of electroneutrality ((Bieniasz, 2004a) and (Bieniasz, 2004b)). More examples about the *h*-refinement are found in (Lang, 1998, Wang et al., 2004, Trompert and Verwer, 1991).

Probably the most significant adaptive mesh technique regarding our work is the algorithm suitable for modeling the transient behavior of the same system with completely different boundary conditions (Přibyl et al., 2006). This method is attached to the commercial FEMLAB routines, which are based on the finite element method. Their monitor function is derived from the spatial derivatives of hydrogen, hydroxyl ion concentrations and the potential. Due to the time-consuming evaluation of the monitor function and successive mesh adaptation, the evaluation is not carried out at each time integration step, the adaptation and consecutive evaluation time interval is determined based on the estimation of transport times.

1.1. Aim of this work

In this paper we would like to report our empirical moving mesh method (*r*-refinement), which was developed to model the time-dependent salt-effects of an electrolyte diode. The algorithm is attached to the commercial COMSOL equation-based modeling software, which provides the spatial and time discretization FEM algorithms with well-defined interfaces. The main idea of this method is, that in a reaction-diffusion system, where reaction fronts move, the local reaction rate indicating the presence of any chemical reaction can be the basis of an adaptive mesh refinement. The problematic part of such a system is the neighborhood of the local chemical reactions, where the gradients and the numerical error of approximation are the highest. This idea could be the basis of any spatial discretization method, not only the finite element method, the advantages would be the same: easy implementation, simple monitor function, hence the required mesh density would be determined in an empirical way not directly derived from the error of approximation.

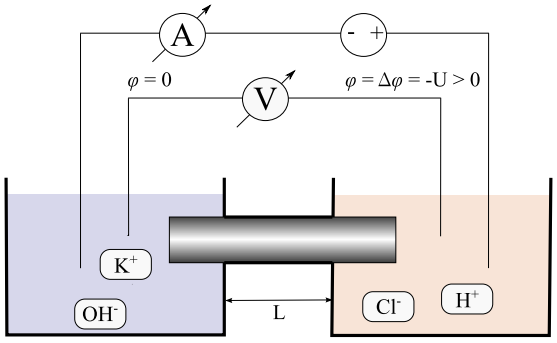

Fig. 1. Schematic view of a strong acid-base diode: An alkaline reservoir (filled by e.g. 0.1 M KOH solution) and an acidic one (filled by e.g. 0.1 M HCl solution) are connected by a hydrogel. $\Delta\varphi > 0$ means reverse biased diode, the opposite is forward biased.

2. Numerical simulations

2.1. The model

The so-called acid-base diode (or electrolyte diode) is a reaction - diffusion - ion-migration system (Noszticzius and Schubert, 1973, Schubert and Noszticzius, 1977), where, due to the applied potential and concentration gradients, the chemical species move, while an acid-base reaction occurs. Previously some highly nonlinear phenomena called positive and negative salt effects related to the salt-contamination of the acid-base diode were discovered, thus it is straightforward to use the negative salt effect to sensitively detect nonhydrogen cations (Chun and Chung, 2015, Roszol et al., 2010, Kirschner et al., 1998).

In an acid-base diode a connecting element (either a hydrogel or a membrane) connects an alkaline (KOH) and an acidic (HCl) reservoir, restraining convection, but allowing diffusion, migration and chemical reaction. (The schematic view of an acid-base diode is shown in Fig. 1) If the acidic reservoir has a negative potential in comparison to the alkaline one (forward biased diode), from the alkaline reservoir cations (e.g. K^+), from the acidic one anions (e.g. Cl^-) can migrate into the gel cylinder, where they form a well-conducting salt (in this case KCl). If the acidic reservoir is the positive side (reverse biased diode), hydrogen (H^+) and hydroxil (OH^-) ions can move into the hydrogel, where water is formed from their reaction, resulting in much smaller conductivity.

Most gels contain fixed weakly acidic groups. The dissociation of them leads to fixed negative ions, in the present work FA^- is the fixed charge, and HFA denotes its protonated form. The current - voltage characteristic of an electrolyte diode resembles to the characteristic of a semiconductor one, meaning the diode current depends on the polarity of the applied voltage, as Fig. 2 shows.

If the reservoirs of the diode are contaminated by a salt (in the case of strong diode by KCl), the concentration of the contaminating salt influences the current of the reverse biased diode:

- If only one reservoir is contaminated (usually the alkaline one due to higher sensitivity), the diode current increases in a nonlinear way (Fig. 3/a). This phenomenon is called positive salt-effect ((Kirschner et al., 1998, Hegedűs et al., 1999)).
- If one side of the diode is already contaminated, and the opposite reservoir of the diode gets contaminated as well, surprisingly the

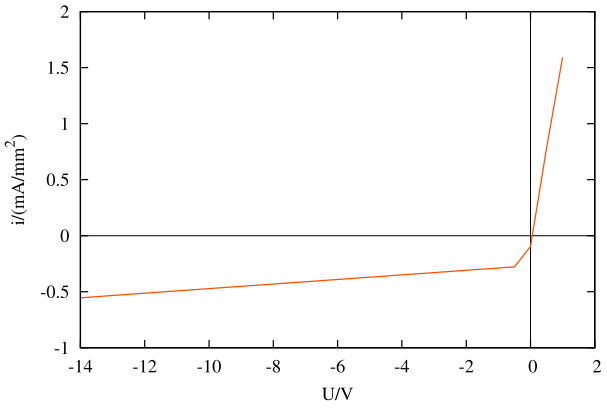

Fig. 2. Simulated voltage – current density characteristic of a strong acid-base diode. Concentrations of the electrolytes: [KOH] = [HCl] = 0.1 M.

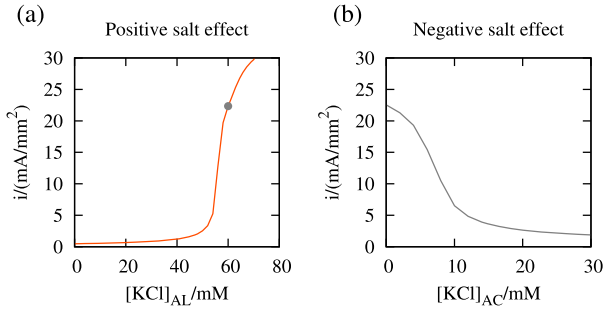

Fig. 3. Calculated current density as the function of salt contamination. (a): positive salt effect, (b): negative salt effect. $[KCl]_{AL}$ and $[KCl]_{AC}$ denote the salt concentration in the alkaline and acidic reservoirs, respectively. The black dot in subfigure (a) represents the alkaline salt concentration used for subfigure (b). $[KCl]_{AL} = 60$ mM, $\Delta\varphi = 10$ V.

diode current decreases by increased counter salt contamination (Fig. 3/b). This phenomenon is called negative salt-effect.

Both positive and negative salt effects had already been investigated for stationary state (Kirschner et al., 1998, Roszol et al., 2010), we started to focus on the time-dependent modeling of salt-contaminated diode (Koncz et al., 2017), where we met unexpected computational complexity.

At this stage of investigation, the mathematical model of the diode is a system of one-dimensional partial differential equations (Roszol et al., 2010, Merkin et al., 2000, Hegedűs et al., 1996, Lindner et al., 2002). The previously discussed simplifications and assumptions ((Iván et al., 2002)) are kept (one dimensional model, concentration polarization and ohmic potential drop on the reservoir are neglected).

To calculate the concentration distribution of the i-th component the mass-balance equation is used, and the Nernst-Planck equation is used to obtain the current density:

$$\frac{\partial c_i}{\partial t} = -\frac{\partial}{\partial x}\left(-D_i\frac{\partial c_i}{\partial x} - \frac{z_i D_i F}{RT}c_i\frac{\partial \varphi}{\partial x}\right) + \sigma_i, \tag{1}$$

where c_i, z_i and D_i denote the concentration, charge number and diffusion coefficient of the i-th component (H^+, OH^-, K^+, Cl^-, FA^-, HFA), respectively. T is the temperature, F is the Faraday constant, R is the molar gas constant, φ denotes the space dependent potential, t is the time coordinate and x is the space coordinate along the connecting element. σ_i denotes the reaction rate of the i-th chemical component:

$$\sigma_{H^+} = k_w(K_w - c_{H^+}c_{OH^-}) + k_f(K_f c_{HFA} - c_{H^+}c_{FA^-}), \tag{2}$$

$$\sigma_{OH^-} = k_w(K_w - c_{H^+}c_{OH^-}), \tag{3}$$

$$\sigma_{K^+} = \sigma_{Cl^-} = 0, \tag{4}$$

$$\sigma_{FA^-} = -\sigma_{HFA} = k_f(K_f c_{HFA} - c_{H^+}c_{FA^-}), \tag{5}$$

where K_w is the equilibrium constant of water dissociation, and k_w denotes the rate constant of water recombination. K_f is the dissociation constant and k_f denotes the kinetic constant of the fixed charge.

Poisson equation is used to calculate the potential profile of the diode:

$$\frac{\partial}{\partial x}\left(-\varepsilon\frac{\partial \varphi}{\partial x}\right) = F\left(\sum_i z_i c_i\right), \tag{6}$$

where ε denotes the permittivity of water.

In our model calculations Dirichlet boundary conditions were applied. Donnan equilibrium is used to calculate the constant boundary concentrations inside the connecting element from the fixed concentrations in the reservoirs. The Donnan potential was used to correct the electric potential.

Unfortunately we were not able to reach convergence, if the above discussed full system of differential equations is applied (mass balance equations are set up for each species). For stationary investigations the concentration of the fixed anions can be calculated from the equilibrium,

$$c_{FA^-} = \frac{c_f}{c_{H^+}/K_f + 1}, \tag{7}$$

where c_f denotes the estimated total concentration of the fixed groups (Iván et al., 2004), therefore the mass-balance equation is used for the mobile ions (H^+, OH^-, K^+, Cl^-) only.

This assumption of quasi-stationarity was considered to be valid even in time dependent cases The usage of this simplification means that the protonation and deprotonation of the fixed charge groups are considered instantaneous, thus the reaction rate belonging to the fixed groups is approximated by zero ($\sigma_{FA^-} = \sigma_{HFA} = 0$). The remaining reaction rate of H^+ is: $\sigma_{H^+} = \sigma_{OH^-} = k_w(K_w - c_{H^+}c_{OH^-})$.

With this simplification it becomes possible to solve the remaining PDEs with COMSOL.

The applied values of the parameters can be found in Table 1.

2.2. Solution method with COMSOL

The simulations were carried out by using the commercial FEM software package COMSOL Multiphysics 4.3. The model was defined from the following interfaces: for the Nernst-Planck equation the "Transport of Diluted Species" and "Classical PDEs/Poisson equation" were applied. A full model calculation can be split into two main steps: after computing the boundary conditions, the initial conditions (this is a stationary state of the diode) are calculated by a previously discussed parametric stationary solver (Roszol et al., 2010), which is followed by the time-dependent study. The solver settings are adjusted under the "Study" node, where the two study steps belonging to the solvers are defined. Between the two study steps the boundary conditions must be reset for the transient value. (In the case of step 1 *Compute to selected*, in the case of step 2 *Compute from selected* command must be used.)

For the numerical integration of the time-dependent ODEs (after spatial discretization) BDF method with SPOOLES linear solver was applied with the following settings: automatic scaling, the time-steps are determined freely by the solver. To avoid numerical oscillations crosswind diffusion stabilization technique was applied. Second order Lagrange elements were used.

The key of FEM simulations is the applied mesh. The gradients of the concentrations and potential are the largest in the neighborhood of the so-called reaction zone, this is the hardest to calculate part of an acid-base diode. To achieve convergence, in this zone extremely fine mesh is required. During the time-dependent study the location of the reaction zone is changing, hence an adaptive meshing technique is highly recommended to reduce computational costs.

In COMSOL Multiphysics adaptive mesh refinement extension is available for the time-dependent studies. Unfortunately this built-in tool

Table 1. Model parameters (Marcus (1997)).

c_{KOH} (moldm^{-3})	Concentration of base	0.1
c_{HCl} (moldm^{-3})	Concentration of acid	0.1
D_{H^+} (m^2 s^{-1})	Diffusion coefficient of protons	9.31×10^{-9}
D_{OH^-} (m^2 s^{-1})	Diffusion coefficient of hydroxyl ions	5.28×10^{-9}
D_{K^+} (m^2 s^{-1})	Diffusion coefficient of potassium ions	1.96×10^{-9}
D_{Cl^-} (m^2 s^{-1})	Diffusion coefficient of chloride ions	2.04×10^{-9}
D_{FA^-} (m^2 s^{-1})	Diffusion coefficient of the fixed charge	0
D_{HFA} (m^2 s^{-1})	Diffusion coefficient of the protonated fixed group	0
φ_L (V)	Electric potential on the L boundary	0
φ_R (V)	Electric potential on the R boundary	$10 - 20$
l (m)	Length of the gel	1×10^{-3}
z_{H^+}	Charge number of protons	1
z_{OH^-}	Charge number of hydroxyl ions	-1
z_{K^+}	Charge number of potassium ions	1
z_{Cl^-}	Charge number of chloride ions	-1
z_{FA^-}	Charge number of the fixed charge	-1
z_{HFA}	Charge number of the protonated fixed charge	0
F (Cmol^{-1})	Faraday constant	9.6487×10^4
R (Jmol^{-1} K^{-1})	Molar gas constant	8.314
T (K)	Temperature	298.15
ε (AsV^{-1} m^{-1})	Permittivity of water	6.954×10^{-10}
k_w (m^3 mol^{-1} s^{-1})	Kinetic constant of water recombination	1.3×10^8
K_w (mol^2 m^{-6})	Ionic product of water	1×10^{-8}
c_f (molm^{-3})	Concentration of the fixed charge	4
k_f (m^3 mol^{-1} s^{-1})	Kinetic constant of the fixed charge	6×10^6
K_f (molm^{-3})	Dissociation constant of the fixed charge	1×10^{-1}

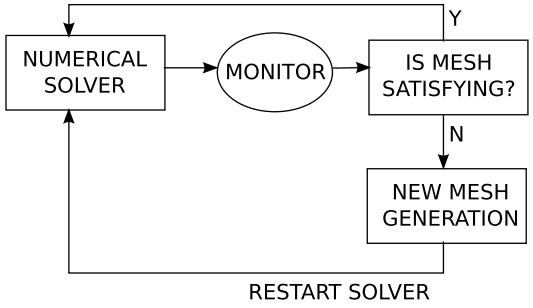

Fig. 4. The general operation of adaptive meshing algorithms.

and the COMSOL's Moving Mesh interface proved to be inadequate for our purposes. Thus we attached an own adaptive algorithm to our simulation framework. (Carrying out model calculations in COMSOL GUI in series is cumbersome, therefore an easy-to-use framework was developed in Java using the COMSOL Java API.)

For the general operation of adaptive meshing algorithms see Fig. 4. The numerical solver must be monitored, and at the end of every iteration step it must be decided, whether the iteration can be continued (mesh is still satisfying) or a new mesh should be generated. In case of a new mesh the last solution with the old mesh is interpolated to the new one, and the numerical solver is restarted. In COMSOL the FEM algorithms are considered to be "black boxes", that is the numerical method can be reached only via the interfaces provided by COMSOL. To stop and monitor the numerical solver, a stop condition is formulated applying the so-called "Domain Point Probe". With a point probe expression a function of variables of the differential equation at a pre-defined location is evaluated.

At the two edges of the reaction zone, inside the dense mesh zone, two point probe expressions are defined. The values of them are the absolute value of the acid-base reaction's local reaction rate at the given location:

$$ppv = \left|\sigma_{H^+}\right| = \left|\sigma_{OH^-}\right| = \left|k_w(K_w - c_{H^+}c_{OH^-})\right|. \tag{8}$$

Then the stop condition is the following: if one of the point probe expressions differ significantly from zero ($ppv > 1.3 \cdot 10^{-3} \frac{\text{mol}}{\text{dm}^3\,\text{s}}$), the solver is stopped. This ppv value means the solver stops when $c_{H^+} \cdot c_{OH^-} > K_w$, we get this threshold by trial and error. After that, from the behavior of the reaction zone a new mesh is generated. With COMSOL Java API in the case of one dimensional geometry only the vertex coordinates are calculated, the edges are trivial (how the vertexes are connected to an element). In COMSOL the solution of the time-dependent solver is copied (Copy solution) to retain the results, and the domain point probes are relocated before the time-dependent solver is restarted.

2.3. Adaptive algorithm with grid function

The so-called grid function was selected to define the mesh. An $x \to f(x)$ grid function defines the real mesh's coordinates as a function of the equidistant mesh's coordinates. Some grid functions with schematic one dimensional meshes are shown in Fig. 5.

The basis of our selected grid function is an equidistant mesh with a refined zone (Fig. 5/b), where the vicinity of the reaction zone is covered by an extremely fine mesh. To avoid numerical problems arising from sudden changes in the size of neighboring elements, in the vicinity of the straight line's intersections exponential smoothing functions are applied. For more details see the 1st section of the Supplementary Information.

The adaptive algorithm based on the grid function has the following parameters:

- N: total number of mesh points
- y_A, y_B: in real-mesh coordinates the initial limits of the extremely fine mesh zone
- R: ratio of the number of points between y_A and y_B and the total number of grid points
- δ: width of the exponential smoothing part in equidistant mesh coordinates
- d: distance between y_A or y_B and its corresponding point probe expression
- Δy: how much the control points (y_A, y_B) of the grid function are shifted into the direction of the reaction's movement, after the stop condition is fulfilled, and the next mesh is generated

The main advantage of applying a grid function is its easy implementation, simple mesh generation, and low time-demand of mesh

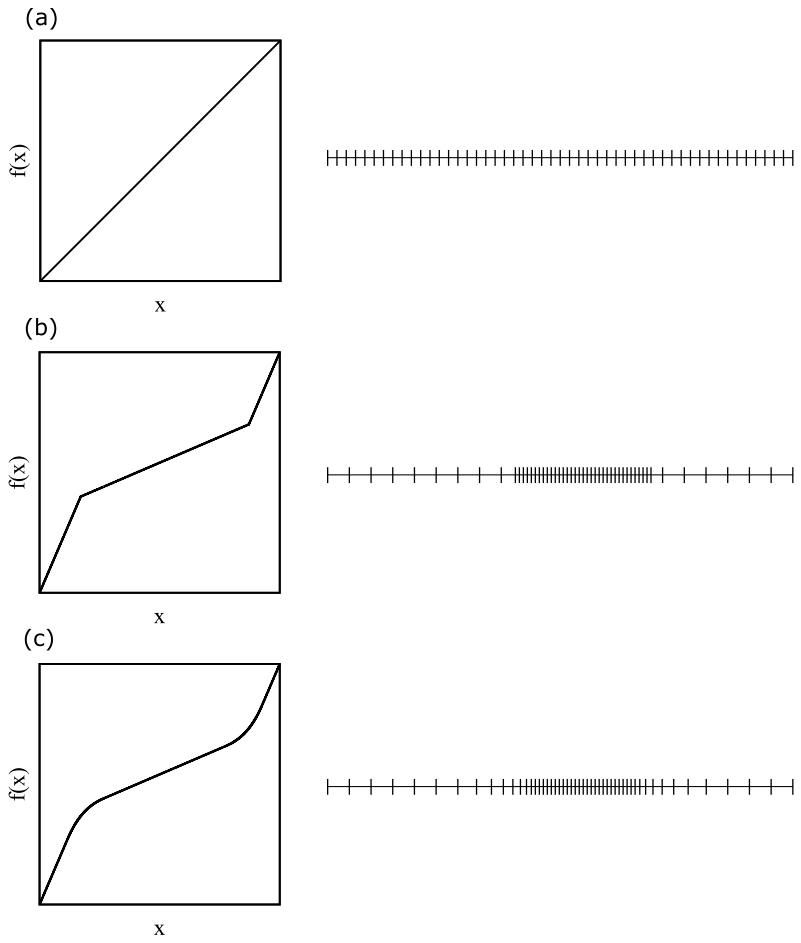

Fig. 5. Some grid functions with the corresponding schematic mesh illustrations. (a) Equidistant mesh. (b) Equidistant mesh with a refined zone. (c) The applied grid function with exponential smoothing.

construction. For the source code see https://github.com/vikikoncz/adaptive_FEM_based_reaction_zone.

3. Results and discussion

We would like to show the ability of the adaptive mesh algorithm to simulate the time-dependent behavior of an acid-base diode. In the present work we demonstrate the operation of the algorithm in case of time-dependent positive salt effect with the following settings. As initial state the salt-free stationary diode was used. The contaminating salt was added to the alkaline reservoir at $t = 0$, $[KCl]_{AL,t} = 60$ mM. Approximately after 100 s the new steady state was attained, thus 150 s was simulated after the system was perturbed by KCl contamination.

Our work is presented in three subsections. First, in Section 3.1 the appearance of the reaction zone is investigated. We would like to show, that the location of the chemical reaction (where the reaction ratio differs significantly from zero) is very close to the location where the gradients of the concentration and potential are the highest.

Then, we investigated the absolute and relative error of approximation on the modeled domain for validation purposes (Section 3.2).

Finally, we discuss the effect of different meshes on the error of approximation and simulation time (Section 3.3).

3.1. Reaction zone

The local reaction rate of the acid-base reaction is $\sigma_{H_2O} = -k_w(K_w - c_{H^+}c_{OH^-})$. It is the linear function of $[H^+] \cdot [OH^-]$, which in equilibrium is a temperature dependent constant. Fig. 6 shows the local reaction rate (σ_{H_2O}) along the gel cylinder in a stationary salt-free diode. σ_{H_2O} is different from zero only at the reaction zone, where the acid-base reaction occurs.

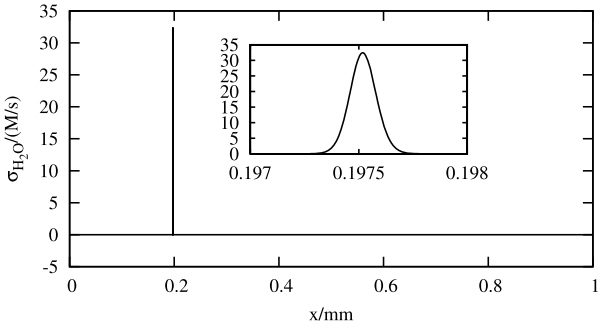

Fig. 6. The local reaction rate ($\sigma_{H_2O} = -k_w(K_w - c_{H^+}c_{OH^-})$) of water recombination in the uncontaminated diode.

Fig. 7 shows some calculated σ_{H_2O} profiles of a time-dependent positive salt effect. At a certain time σ_{H_2O} is different from zero in one region only, certainly this is the reaction zone.

As the alkaline reservoir (left hand side) is approached by the reaction zone, the acid-base reaction becomes faster and faster (the peak of σ_{H_2O} increases). The reaction zone keeps its position after about 10 s, however, the reaction rate continues increasing.

The look of the reaction zone at four selected moments of time is shown in Fig. 8. While the acid-base reaction gets faster, the extension of the reaction zone shrinks. In the new steady state its width is only

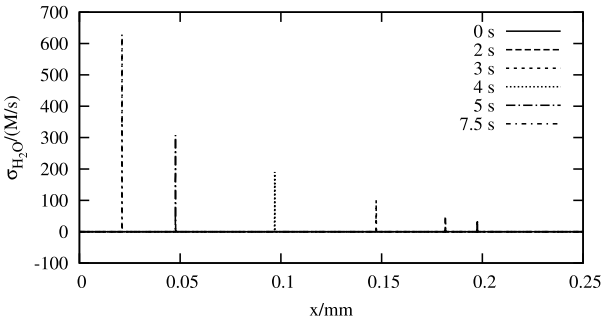

Fig. 7. The local reaction rate ($\sigma_{H_2O} = -k_w(K_w - c_{H^+}c_{OH^-})$) of water recombination at different moments of time.

the third of the uncontaminated one. The extension of the reaction zone is calculated from the half-width of the σ_{H_2O} peak.

In the uncontaminated steady state the positions of the extrema of spatial derivatives are very close to the location where the acid-base reaction occurs. These derivatives move together with the chemical reaction. The local extrema of concentration derivatives are increasing (in absolute value), while the derivative of potential changes only slightly. The situation is the same in the case of second spatial derivatives.

3.2. Validation

In the case of a system of nonlinear partial differential equations, it is possible, that the numerical solver finds a physically invalid solution even though it satisfies the tolerance criteria (LeVeque (1992)). We used a posteriori error indicators to characterize the precisity of the numerical solutions.

A meaningful measure of the computational error can be given on (x_i, x_{i+1}) as follows:

$$\int_{x_i}^{x_{i+1}} (\tilde{y}(x) - y(x))^2 \, dx = R(x, \mathbf{a}), \tag{9}$$

where $y(x)$ denotes the real solution of the differential equation and $\tilde{y}(x) = \sum_{j=1}^{n} a_j \cdot \Phi_j(x)$ is the finite element approximation. In practice, the real solution is unknown, therefore, another error indicator has to be found.

If the coefficients a_j of the basis functions are available, substituting them into the original PDE's leads to an error indicator on each element.

Unfortunately due to COMSOL's 'black box' approach it is neither possible to get the Lagrangian coefficients, nor the error calculated by COMSOL.

To find a metric for comparing different solutions, an own method had to be developed. It is possible to export from COMSOL the interpolated solution, and the spatial and time derivatives of the variables of the equation at the predefined points in a given moment. (From COMSOL Java API the so-called 'Interp' function was applied to retrieve the numerical results.) Our method is the following: during time development at every discrete moment of time the approximated value of the variables, the 1st and 2nd spatial derivatives and the time-derivatives are exported at the mesh points. These values can be substituted to the five differential equations (four mass balances and the Poisson) at every moment and location, leading to five (absolute) residual values $err_{abs,i}$.

As an example, the calculated absolute residual values of the H^+'s mass balance equation, and the Poisson equation are shown in Figs. 9 and 10.

The absolute error in itself does not tell us the whole picture, it has to be compared to the absolute values of the various terms in the given equation. For this reason we use the relative error defined in the following way:

$$err_{rel,i} = \frac{err_{abs,i}}{\left|\frac{\partial c_i}{\partial t}\right| + \left|-\frac{\partial}{\partial x}\left(-D_i\frac{\partial c_i}{\partial x}\right)\right| + \left|-\frac{\partial}{\partial x}\left(-\frac{z_i D_i F}{RT}c_i\frac{\partial \varphi}{\partial x}\right)\right| + |\sigma_i|} \tag{10}$$

$$err_{rel,Poisson} = \frac{err_{abs,Poisson}}{\left|\frac{\partial}{\partial x}\left(-\varepsilon\frac{\partial \varphi}{\partial x}\right)\right| + \left|F\left(\sum_i z_i c_i\right)\right|} \tag{11}$$

Despite of the large absolute error in the neighborhood of the reaction zone, the relative errors (Figs. 11 and 12) seem to be mostly acceptable. However, a very sharp region exists in the middle of the reaction zone, where the approximation error of the Poisson equation becomes 0.65.

3.3. The effect of the grid function's parameters on the error of approximation and on the simulation time

To compare the different types of meshes, the simulation time measured in an isolated virtual machine (for details see the 2nd section of Supplementary Information) was monitored, and the error of approximation was estimated. Unfortunately, the number of iterations are not measurable via COMSOL, thus we had to measure the running time of the simulations. It is also important in practice, but depends on the hardware. The basic steps of an adaptive FEM simulation with the measured running time values are found in the 4th section of Supplementary Information. About 97% of the total simulation time goes to the time-stepping and mesh interpolation, thus the running time of the other stages of FEM simulation is negligible.

Instead of plotting the residuals at every moment of time (like in Section 3.2), it is better to use a cumulated error indicator to describe the applicability of the mesh. To construct such an a posteriori error indicator, we consider equation (1) as a system of conservation laws coupled with the reactive source terms $(\sigma_{H^+}, \sigma_{OH^-}, 0, 0)$. Using the corresponding theory for the non-linear conservation laws in Theorem 5.2 in (Cockburn, 1999), a straightforward choice for the error estimation of the j-th component in equation (1) can be calculated as follows:

$$err_j = \int_0^T \int_0^L |err_{abs,j}| dt dx + \sqrt{\max_{t\in[0,T]} S(c_j)(t) \cdot \int_0^T S(c_j)(t) dt} \cdot \sqrt{D_j}, \tag{12}$$

where $err_{abs,j}$ denotes the j-th components calculated residual, and $S(c_j)(t)$ is the sum of the concentration absolute differences between the grid points on the entire modeled domain. We found, that the term containing S is almost negligible compared to the time and spatial integral of the residuals. Furthermore, it was found that this term varies within 1% in the case of every mesh setting (if convergence is achieved), thus it can be neglected when comparing meshes.

For a single cumulative error indicator the error estimation of the four components is summed and normed by $T = 150$ s (due to the time integration):

$$error = \frac{err_{H^+} + err_{OH^-} + err_{K^+} + err_{Cl^-}}{T}. \tag{13}$$

In the following tables and figures only this cumulative value is used to compare different meshes.

First, the efficiency of the adaptive meshing algorithm is showed with comparison to two fixed mesh simulations. After that, the effects of the grid function parameters are explored, and we tried to find an optimal parameter combination considering the simulation time and the error of approximation. (In this study the parameters are fixed during a simulation.) Finally, we investigated how the continuous modification of the grid function's parameters influences the simulation.

3.3.1. Fixed mesh vs adaptive mesh

The performance of an equidistant mesh (named fixed(1)), a fixed mesh with a dense zone (fixed(2)) and three moving meshes with the proposed grid function were compared (Table 2). The running time of

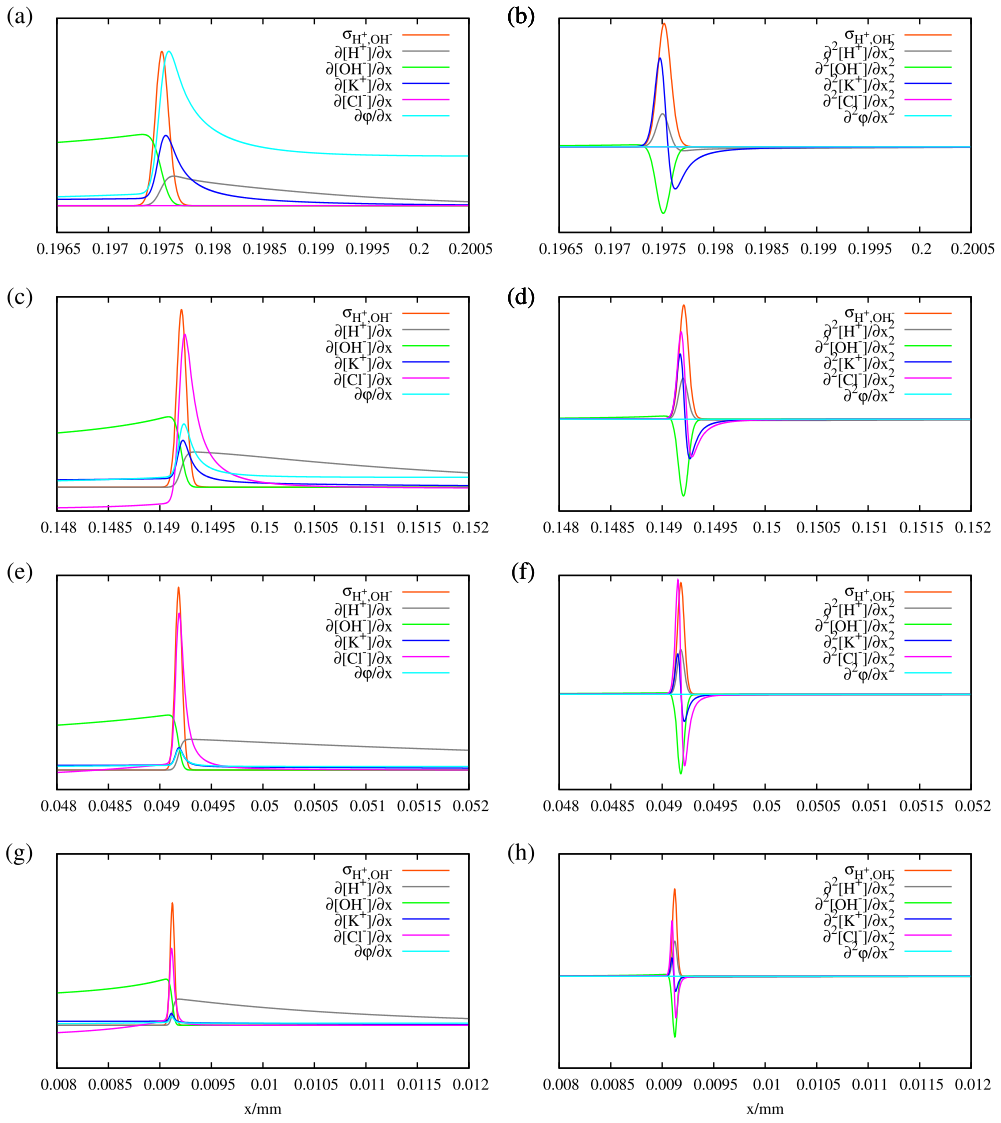

Fig. 8. Reaction fronts: spatial gradients and the local reaction rate of acid-base reaction in different moments of time. In the first column the local reaction rate and the 1st spatial derivatives are shown at t = 0 s (a), t = 3 s (c), t = 5 s (e) and t = 20 s (g). In the second column the local reaction rate and the 2nd spatial derivatives are shown at t = 0 s (b), t = 3 s (d), t = 5 s (f) and t = 20 s (h), respectively. Please note: the derivatives and the local reaction rate are scaled, thus no unit is shown in this figure, because we are only interested in the positions of peaks, not their magnitude.

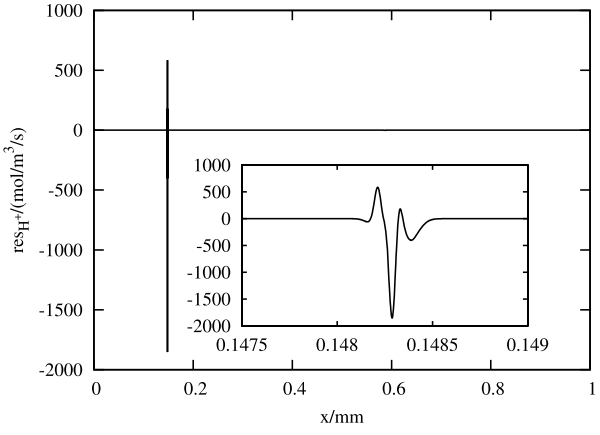

Fig. 9. The absolute error of the H^+ ions mass balance equation (err_{abs,H^+}) at $t = 3$ s. The parameters of the applied mesh are the following: $N = 10000$, $y_A = 0.192$, $y_B = 0.202$, $d = 0.002$, $\Delta y = 0.002$, $\delta = 0.01$, $R = 0.8$.

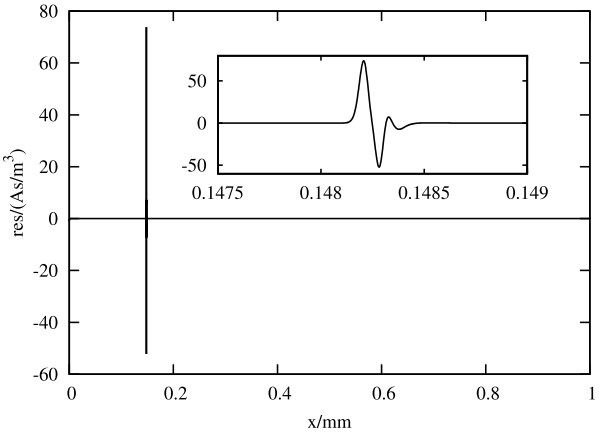

Fig. 10. The absolute error of the Poisson equation ($err_{abs,Poisson}$) at $t = 3$ s. The parameters of the applied mesh are the following: $N = 10000$, $y_A = 0.192$, $y_B = 0.202$, $d = 0.002$, $\Delta y = 0.002$, $\delta = 0.01$, $R = 0.8$.

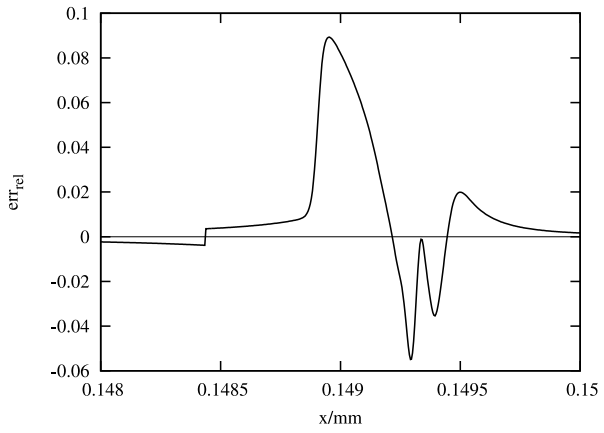

Fig. 11. The relative error of the H^+ ions mass balance equation (err_{rel,H^+}) at $t = 3$ s in the reaction zone. The parameters of the applied mesh are the following: $N = 10000$, $y_A = 0.192$, $y_B = 0.202$, $d = 0.002$, $\Delta y = 0.002$, $\delta = 0.01$, $R = 0.8$.

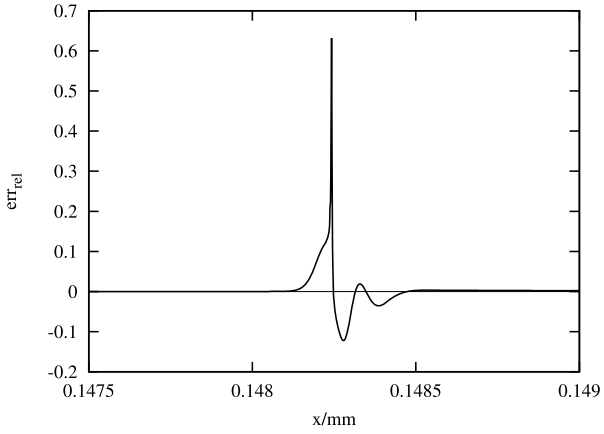

Fig. 12. The relative error of the Poisson equation ($err_{rel,Poisson}$) at $t = 3$ s in the reaction zone. The parameters of the applied mesh are the following: $N = 10000$, $y_A = 0.192$, $y_B = 0.202$, $d = 0.002$, $\Delta y = 0.002$, $\delta = 0.01$, $R = 0.8$.

Table 2. The measured running time and calculated error of approximation (error) in the case of fixed and adaptive meshes. The fixed(1) mesh is an equidistant mesh, fixed(2) is a fixed mesh with a dense zone. Parameters of the grid function are the following: $y_A = 0.192$, $y_B = 0.202$, $d = 0.002$, $\Delta y = 0.002$, $\delta = 0.01$, $R = 0.8$.

Mesh type	N	Time (min)	error
fixed(1)	100000	3648	147
fixed(2)	21000	532	73
adaptive	500	15	183
adaptive	1000	35	97
adaptive	2000	42	49
adaptive	10000	222	10

the equidistant mesh (10000 grid points) is the biggest, and approximately the same precision can be achieved using an adaptive mesh with 500 - 1000 grid points depending on the grid function parameters.

The fixed(2) mesh has the same resolution as the equidistant mesh (fixed(1)) in its dense part, which covers that part of the gel, where the reaction zone can occur. The remaining part of the gel is covered by an 80 times less dense equidistant mesh, and the two zones are connected by an exponential smoothing part.

Despite the same resolution in the reaction zone, the error of approximation is almost halved in the case of fixed(2), due to the convergence

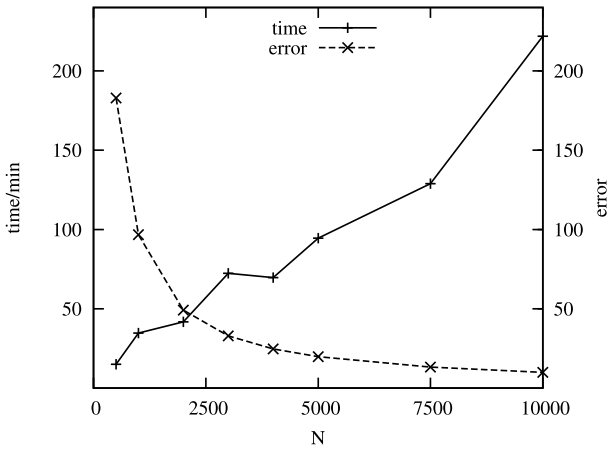

Fig. 13. The measured running time and the error of approximation as the function of the number of grid points. Parameters of the grid function are the following: $y_A = 0.192$, $y_B = 0.202$, $d = 0.002$, $\Delta y = 0.002$, $\delta = 0.01$, $R = 0.8$.

criteria of COMSOL's nonlinear solver. In the aggregated error evaluated by COMSOL after every iteration step, the error on an element is not weighted by the element's size. Thus in COMSOL's aggregated error, in the case of equidistant mesh the elements belonging to the reaction zone are underweighted compared to the fixed(2) mesh. (Further details about COMSOL's convergence criteria can be found in the 3rd section of the Supplementary Information.)

The most accurate solution is achievable by a moving mesh with as many grid points as the desired running time allows. (In our case maximum 10000 mesh elements were used.) In the case of one specific adaptive mesh parameter setting the measured running time and the error of approximation as the function of the number of grid points are shown in Fig. 13. (Mesh trajectories of this moving mesh can be found in the 7th section of the Supplementary Information.)

If the number of grid points increases, the approximation error decreases in a hiperbolic way. The running time can show discrepancies, it does not increase monotonically as a function of N.

The convergence rates of these discretization schemes (fixed(2), and adaptive) are compared in the 6th section of the Supplementary Information.

3.3.2. *The effect of the grid function parameters*

In this section we present our findings about systematic investigations of the effect of grid function parameters on the performance of the moving mesh algorithm. Please note, during one simulation the parameters of the grid function were kept constant. During the discovery of the parameters $N = 2000$ was chosen, because we found it a good compromise between running time and error of approximation (see Table 2).

First, the effect of Δy was investigated (Fig. 14). It does not influence the error of approximation significantly, however, the measured simulation time depends on it. The smaller the Δy is, the higher the running time becomes. The frequent mesh adaptation needs too much interpolation between the different meshes.

Within a wide range the grid function parameter called R has very similar effect on the error and simulation time (Fig. 15). If R is too small, the solver just cannot converge (because the resolution is not high enough in the reaction zone). Certainly, the precise value depends on the number of grid points, and the other parameters of the grid function, e.g. if $N = 2000$, R must be at least 0.05. However, in this case the approximation error is huge (2600). (For this reason it is not shown in Fig. 15.) The error of approximation has an optimum around $R = 0.94$, if R is larger, too few grid points appear outside the reaction zone.

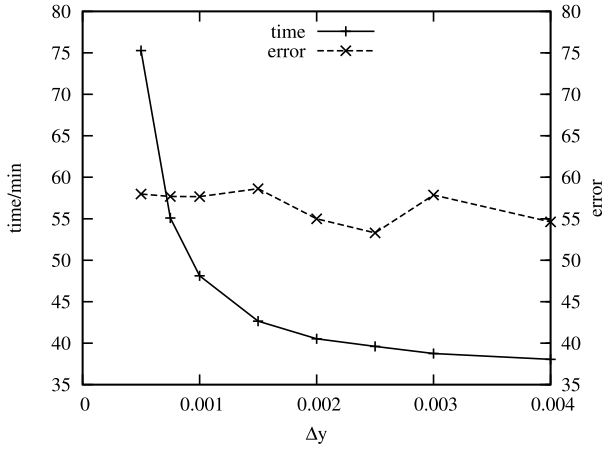

Fig. 14. The measured running time and the error of approximation as the function of the Δy parameter. Parameters of the grid function are the following: $y_A = 0.191$, $y_B = 0.203$, $d = 0.003$, $R = 0.8$, $\delta = 0.01$, $N = 2000$.

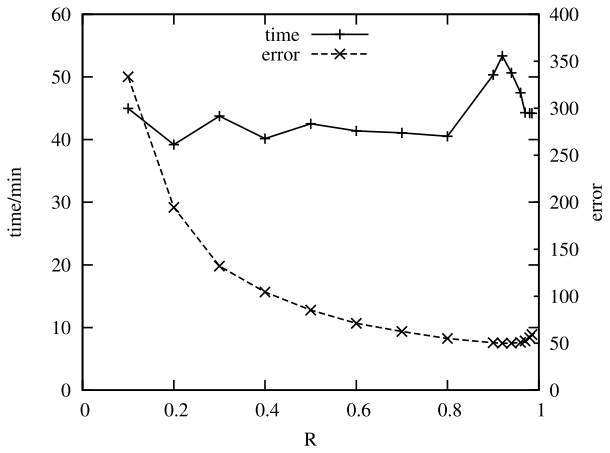

Fig. 15. The measured running time and the error of approximation as the function of the R parameter. Parameters of the grid function are the following: $y_A = 0.191$, $y_B = 0.203$, $d = 0.003$, $\Delta y = 0.002$, $\delta = 0.01$, $N = 2000$.

Depending on the width of the extremely fine mesh zone, and on the grid function parameters, an optimal δ exists, where the error of approximation is the smallest (Fig. 16). If δ increases from zero, first the error of approximation decreases, due to smoother transition of element size. When δ becomes comparable to the size of the dense mesh zone, the number of mesh elements in the reaction zone starts to decrease, resulting in increased error of approximation.

Due to the time demand of too frequent mesh adaption, and due to convenience, dense mesh was usually used on a large environment of the reaction zone. (It means, $y_B - y_A$ is at least five times bigger, than the reaction zone's extension.) The impact of the distance between y_A and y_B was investigated (Fig. 17) to see whether covering a smaller environment with dense mesh still gives satisfactory results. The error of approximation increases with this distance (because less grid elements cover the reaction zone). Usually smaller error comes with lower running time, however, here the opposite happens: increased error decreases the running time.

The minimal reasonable distance between y_B and y_A is the extension of the reaction zone: under this limit convergence problems appear. In the case of minimal $y_B - y_A$ the error and the running time as the function of N is shown in Fig. 18. To reach convergence with these settings, the minimum number of required elements is $N = 150$, although in this case the error of approximation is around 450, and the profiles are not smooth enough. If $N = 500$, the algorithm has very similar performance, as $N = 2000$ with the widely covered zone.

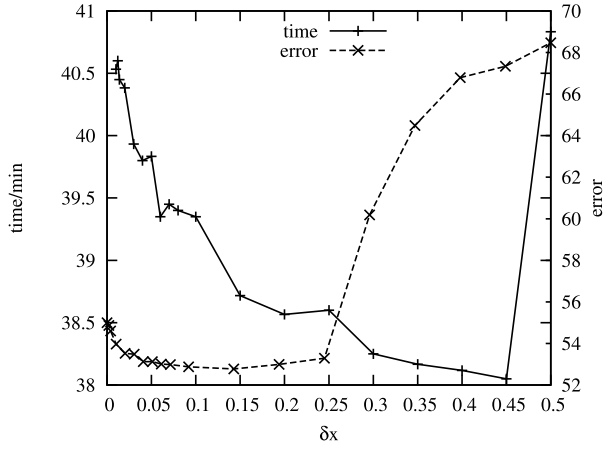

Fig. 16. The measured simulation time and the error of approximation as the function of the δ parameter. Parameters of the grid function are the following: $y_A = 0.191$, $y_B = 0.203$, $d = 0.003$, $\Delta y = 0.002$, $R = 0.8$, $\delta = 0.01$, $N = 2000$.

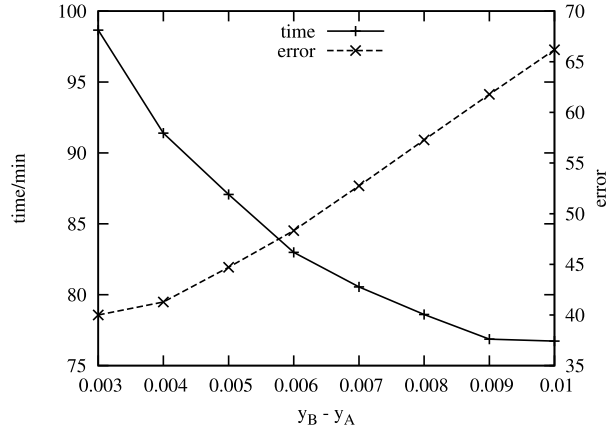

Fig. 17. The measured running time and the error of approximation as the function of the distance between y_A and y_B. Parameters of the grid function are the following: $d = 0.0005$, $\Delta y = 0.0005$, $R = 0.8$, $\delta = 0.01$, $N = 2000$.

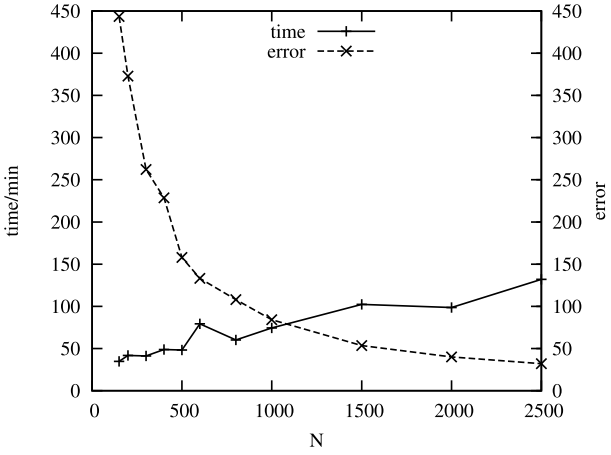

Fig. 18. The measured running time and the error of approximation as the function of the N. Parameters of the grid function are the following: $y_A = 0.196$, $y_B = 0.199$, $d = 0.0005$, $\Delta y = 0.0005$, $R = 0.8$, $\delta = 0.01$. The dense mesh barely covers the reaction zone.

Table 3. The measured running time and the error of approximation in the case of moving mesh algorithms with different continuously modified grid functions. Initial values of the grid function parameters: $N = 10000$, $y_A = 0.191$, $y_B = 0.203$, $d = 0.003$, $R = 0.8$, $\Delta y = 0.002$, $\delta = 0.01$. In the method called CMG 1 only the distance between $y_B - y_A$, d, and Δy are decreased. In the method called CMG 2 R is also decreased, furthermore in the method called CMG 3 even δ is decreased. In the case of NMG (non-modified grid algorithm) the initial values of the parameters are the same, and are kept constant during the simulation.

Mesh type	Time (min)	error
CMG 1	233	7
CMG 2	235	14
CMG 3	257	17
NMG	283	11

3.3.3. *Continuous modification of the parameters*

During the transition of the diode the extension of the reaction zone shrinks. In the new steady state, it's extension is one third, than in the salt free diode (section 3.1). Is it possible to reach better performance by shrinking the fine mesh zone with the reaction zone?

To alter the grid function continuously, the previously discussed algorithm is modified: if the stop condition defined in COMSOL is fulfilled and the iteration stops, then the dependent variables (and its spatial derivatives) must be retrieved at the grid points. The half width of the local reaction rate peak was used to estimate the reaction zone's extension, from which not only the location of the fine mesh zone, but other parameters of the grid function could be re-calculated (for further details see 5th section of Supplementary Information). Unfortunately if the total number of grid points is too small, the estimation of shrinkage of the reaction zone becomes unprecise, leading to non-converging mesh. It means, that in the case of small N continuous modification of the parameters can be numerically unstable.

The performance of algorithms with continuously modified grid (CMG) and a non modified grid (NMG) is summarized in Table 3. The method called CMG 1, where only $y_B - y_A$, d and Δy are shrinked, gives the smallest error and simulation time.

4. Conclusions and outlook

4.1. Conclusions

We suggest an empirical moving mesh algorithm, which was attached to the commercial FEM solver COMSOL. Realizing that higher reaction rate and higher concentration usually appear close to each other, the local reaction rate was used to control the mesh adaption. The proposed algorithm was tested for a reaction-diffusion system called acid-base diode, and the parameters were fine-tuned for this case. During the time-dependent modeling of the so-called salt effects in this system we experienced high computational complexity, thus an adaptive meshing algorithm was necessary to reduce the time of the simulation. We found, that using the local reaction rate instead of the spatial derivatives makes the implementation of the algorithm very easy and simple.

4.2. Outlook

The moving mesh algorithm can be extended to handle the appearance and disappearance of the reaction zones. If the time-dependent solver is stopped, or after every iteration step, the modeled domain can be scanned with a monitor function, which evaluates the local reaction rates, and marks the location of the reaction zone. From the locations a new grid function can be created, in which the less steep straight segments of the piecewise grid function correspond to the reaction zones. (The exponential smoothing, and handling of too close reaction zones need to be dealt with.)

Unfortunately, a straightforward extension of the proposed process for two-dimensional geometric setup seems to be impossible. For such cases, the grid-transformation between consecutive time steps is obtained from the solution of so-called moving mesh PDE (Zegeling et al., 2005). The mesh has to be regularized in many cases and an interpolation is also necessary between two consecutive meshes. For many applications, however, one-dimensional situations are also of great importance.

Furthermore, the local reaction rate can be used as a 'monitor function' not only in r-refinement, but in h-refinement, p-refinement or hp-refinement methods as well. In such cases, in the neighborhood of the chemical reaction mesh elements can be added (and later removed), or the polynomial degree of the basis function can be increased (and later decreased). These techniques are easier to extend to two or more dimensional problems simulated by finite element or finite difference methods.

Declarations

Author contribution statement

Viktória Koncz & Kristóf Kály-Kullai: Conceived and designed the analysis; Analyzed and interpreted the data; Wrote the paper. Ferenc Izsák: Conceived and designed the analysis; Wrote the paper. Zoltán Noszticzius: Contributed analysis tools or data; Wrote the paper.

Funding statement

This work was supported by OTKA Grant K131425 and by the ELTE Institutional Excellence Program (1783-3/2018/FEKUTSRAT) through the Hungarian Ministry of Human Capacities.

Data availability statement

Data will be made available on request.

Declaration of interests statement

The authors declare no conflict of interest.

Additional information

Supplementary content related to this article has been published online at https://doi.org/10.1016/j.heliyon.2020.e05842.

Acknowledgements

The authors thank A. Pataricza for helpful discussions.

References

Bieniasz, L.K., 2000. Use of dynamically adaptive grid techniques for the solution of electrochemical kinetic equations: part 5. A finite-difference, adaptive space/time grid strategy based on a patch-type local uniform spatial grid refinement, for kinetic models in one-dimensional space geometry. J. Electroanal. Chem. 481 (2), 115–133.

Bieniasz, L.K., 2004a. Use of dynamically adaptive grid techniques for the solution of electrochemical kinetic equations. Part 14: extension of the patch-adaptive strategy to time-dependent models involving migration-diffusion transport in one-dimensional space geometry, and it. J. Electroanal. Chem. 565 (2), 251–271.

Bieniasz, L.K., 2004b. Use of dynamically adaptive grid techniques for the solution of electrochemical kinetic equations. Part 15: patch-adaptive simulation of example transient experiments described by Nernst–Planck–electroneutrality equations in one-dimensional space geometry. J. Electroanal. Chem. 565 (2), 273–285.

Cao, W., Huang, W., Russell, R.D., 2003. Approaches for generating moving adaptive meshes: location versus velocity. Appl. Numer. Math. 47 (2), 121–138.

Chun, H., Chung, T.D., 2015. Iontronics. Annu. Rev. Anal. Chem. 8, 441–462.

Cockburn, B., 1999. The Graduate Student's Guide to Numerical Analysis '98. Springer, Berlin.

Coimbra, M.D.C., Sereno, C., Rodrigues, A., 2004. Moving finite element method: applications to science and engineering problems. Comput. Chem. Eng. 28 (5), 597–603.

Farmaga, I., Shmigelskyi, P., Spiewak, P., Ciupinski, L., 2011. Evaluation of computational complexity of finite element analysis. In: 2011 11th International Conference the Experience of Designing and Application of CAD Systems in Microelectronics (CADSM), pp. 213–214.

Hegedűs, L., Kirschner, N., Wittmann, M., Simon, P., Noszticzius, Z., Amemiya, T., Ohmori, T., Yamaguchi, T., 1999. Nonlinear effects of electrolyte diodes and transistors in a polymer gel medium. Chaos 9 (2), 283–297. http://www.ncbi.nlm.nih.gov/pubmed/12779826.

Hegedűs, L., Wittmann, M., Kirschner, N., Noszticzius, Z., 1996. Reaction, diffusion, electric conduction and determination of fixed ions in a hydrogel. Prog. Colloid & Polym. Sci. 102, 101–109.

Huang, W., Ren, Y., Russell, R.D., 1994. Moving mesh partial differential equations (MMPDES) based on the equidistribution principle. J. Numer. Anal. 31 (3), 709–730.

Iván, K., Kirschner, N., Wittmann, M., Simon, P.L., Jakab, V., Noszticzius, Z., Merkin, J.H., Scott, S.K., 2002. Direct evidence for fixed ionic groups in the hydrogel of an electrolyte diode. Phys. Chem. Chem. Phys. 4 (8), 1339–1347.

Iván, K., Wittmann, M., Simon, P.L., Noszticzius, Z., Vollmer, J., 2004. Electrolyte diodes and hydrogels: determination of concentration and pK value of fixed acidic groups in a weakly charged hydrogel. Phys. Rev. E 70 (6 1), 061–402.

Kirschner, N., Hegedűs, L., Wittmann, M., Noszticzius, Z., 1998. Nonlinear "salt-effect" in an electrolyte diode. Theory and experiments. ACH- Models Chem. 135, 279–286.

Koncz, V., Noszticzius, Z., Roszol, L., Kály-Kullai, K., 2017. Time-dependent modeling of salt-contaminated acid-base diodes. J. Electrochem. Soc. 164 (4), H257–H265. http://jes.ecsdl.org/lookup/doi/10.1149/2.1701704jes.

Lang, J., 1998. Adaptive FEM for reaction—diffusion equations. Appl. Numer. Math. 26 (1–2), 105–116.

LeVeque, R.J., 1992. Numerical Methods for Conservation Laws. Birkhäuser, Basel.

Lindner, J., Šnita, D., Marek, M., 2002. Modelling of ionic systems with a narrow acid–base boundary. Phys. Chem. Chem. Phys. 4 (8), 1348–1354.

Marcus, Y., 1997. Ion Properties. Marcel Dekker, New York.

Merkin, J.H., Simon, P.L., Noszticzius, Z., 2000. Analysis of the electrolyte diode. Electrodiffusion and chemical reaction within a hydrogel reactor. J. Math. Chem. 28, 43–58.

Noszticzius, Z., Schubert, A., 1973. "Electrolyte diode" analysis of isothermal transport processes in the interfaces of aqueous solutions. Period. Polytech., Chem. Eng. 17, 165–177.

Přibyl, M., Šnita, D., Kubíček, M., 2006. Adaptive mesh simulations of ionic systems in microcapillaries based on the estimation of transport times. Comput. Chem. Eng. 30 (4), 674–685.

Roszol, L., Várnai, A., Lorántfy, B., Noszticzius, Z., Wittmann, M., 2010. Negative salt effect in an acid-base diode: simulations and experiments. J. Chem. Phys. 132 (6), 064902.

Schubert, A., Noszticzius, Z., 1977. Electrolyte diode - an experimental study polarization phenomena at the junction of the aqueous solutions of an acid and a base. Part II. Period. Polytech., Mech. Eng. 21, 279–283.

Schwab, C., 1999. p- and hp- Finite Element Methods. Clarendon Press, Gloucestershire.

Trompert, R.A., Verwer, J.G., 1991. A static-regridding method for two-dimensional parabolic partial differential equations. Appl. Numer. Math. 8 (1), 65–90.

Wang, R., Keast, P., Muir, P., 2004. A high-order global spatially adaptive collocation method for 1-D parabolic PDEs. Appl. Numer. Math. 50 (2), 239–260.

Zegeling, P.A., Blom, J.G., 1992. An evaluation of the gradient-weighted moving-finite-element method in one space dimension. J. Comput. Phys. 103 (2), 422–441.

Zegeling, P.A., de Boer, W.D., Tang, H.Z., 2005. Robust and efficient adaptive moving mesh solution of the 2-D Euler equations. Contemp. Math. 383, 375–386.

Zegeling, P.A., Keppens, R., 2001. Adaptive Method of Lines for Magnetohydrodynamic PDE Models. Adaptive Method of Lines, pp. 117–137.

Zegeling, P.A., Kok, H.P., 2004. Adaptive moving mesh computations for reaction-diffusion systems. J. Comput. Appl. Math. 168 (1–2), 519–528.

Zimmerman, W.B.J., 2006. Multiphysics Modeling with Finite Element Methods. World Scientific Publishing Company, Singapore.